Stabilizing Quantization-Aware Training by Implicit-Regularization on Hessian Matrix

Junbiao Pang¹, Tianyang Cai¹

¹Beijing University Of Technology junbiao_pang@bjut.edu.cn, tianyang_cai@163.com

Abstract

Quantization-Aware Training (QAT) is one of the prevailing neural network compression solutions. However, its stability has been challenged for yielding deteriorating performances as the quantization error is inevitable. We find that the sharp landscape of loss, which leads to a dramatic performance drop, is an essential factor that causes instability. Theoretically, we have discovered that the perturbations in the feature would bring a flat local minima. However, simply adding perturbations into either weight or feature empirically deteriorates the performance of the Full Precision (FP) model. In this paper, we propose Feature-Perturbed Quantization (FPQ) to stochastically perturb the feature and employ the feature distillation method to the quantized model. Our method generalizes well to different network architectures and various QAT methods. Furthermore, we mathematically show that FPQ implicitly regularizes the Hessian norm, which calibrates the smoothness of a loss landscape. Extensive experiments demonstrate that our approach significantly outperforms the current State-Of-The-Art (SOTA) QAT methods and even the FP counterparts.

1 Introduction

Model compression has become an essential requirement for integrating deep models into edge computing devices. The prevalent methods in the domain of model compression include the search for optimal neural architectures [Zoph and Le, 2016], network pruning [Han et al., 2015], and the Deep Neural Network (DNN) quantization [Li et al., 2021a] [Esser et al., 2019]. DNN quantization are categorized into two sub-classes: Post-Training Quantization (PTQ) [Nagel et al., 2020], [Li et al., 2021a], [Wei et al., 2022], [Li et al., 2023b] and Quantization-Aware Training (QAT) [Esser et al., 2019], [Nagel et al., 2022]. PTQ adjusts the quantized model with a limited calibration dataset, bypassing the need for retraining. However, when dealing with low-bit widths, e.g., 2 or 4 bits, PTQ may face a significant drop in performance. Conversely, QAT re-trains or fine-tunes the neural network

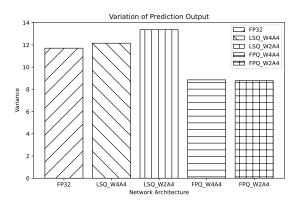


Figure 1: The output variances of FP32, LSQ W4A4, LSQ W2A4, FPQ W4A4, FPQ W2A4 models of the ResNet18 on CIFAR-10 dataset.

to maintain its accuracy especially for an extremely low-bit width model.

Despite QAT tries to preserve the performance of the low bit model by re-training (or fine-tuning) the weights, the stability of a QAT model (*i.e.*, the empirical performance is sensitive to the noise from the input for the quantizated model with the different bit widths) has been challenged. Importantly, the stability of a QAT model is considered to be the empirical way to calibrate the Lipschitz constant of a network [Lin *et al.*, 2019]. That is, if the quantization error occurs, how stable is the output of a neural network?

We have applied Gaussian-distribution perturbations to the original inputs to investigate the stability of the quantized DNN. Fig. 1 illustrates that as the model parameters are optimized, the stability of FP and the SOTA QAT method (LSQ [Esser et al., 2019]) deteriorate. Such instability makes QAT converge to the sharp loss landscape which leads to the significant performance drops when the model is quantized. This phenomenon discovers that the quantized model is highly sensitive to small perturbations from the input [Lin et al., 2019] or the quantization error either from the weights or the activations [Nagel et al., 2019a]. For instance, BENN [Zhu et al., 2019] ensembled multiple binary models to alleviate this problem. However, the inherent instability starts from the QAT training scheme and the ensambling ap-

proach is a compromise with the multiple quantized models for a prediction.

The important sources of such instability come from three dimensions: 1) Straight-Through Estimator (STE)-based QAT has a bias gradient [Shin et al., 2023]; 2) the quantization error would be propagated into the next layer of DNN [Pang et al., 2025]; and 3) the FP model itself is unstable due to the improper Lipsciz constant [Qian and Wegman, 2018]. When these factors appear together for a quantized DNN, there is often a huge performance drop. Given the above factors as $\theta_1, \theta_2, \theta_3$ receptively, the corresponding loss is defined as $L(\theta_1, \theta_2, \theta_3)$. Let $f_{FP}^{(l)}$ and $f_Q^{(l)}$ denote the features at the l-th layer for the FP model and the quantized model, respectively. The quantization would introduce errors into the features as follows:

$$f_{\rm O}^{(l)} = f_{\rm FP}^{(l)} + \Delta f^{(l)}(\theta_1, \theta_2, \theta_3), \tag{1}$$

where $\Delta f^{(l)}(\theta_1,\theta_2,\theta_3)$ represents the perturbation in the feature caused by the factors θ_1,θ_2 and θ_3 at the l-th layer. The perturbation $\Delta f^{(l)}(\theta_1,\theta_2,\theta_3)$ would propagate through all the layers of a neural network, leading to the variance in the final output as follows:

$$L(\theta_1, \theta_2, \theta_3) = L_{\text{original}} + \Delta L(\theta_1, \theta_2, \theta_3), \tag{2}$$

where the $L_{\rm original}$ is from the unperturbed model, and $\Delta L(\theta_1,\theta_2,\theta_3)$ represents the loss caused by about three factors. The perturbation in loss $\Delta L(\theta_1,\theta_2,\theta_3)$ is the errors between the quantized features and the FP features at each layer, which is controlled by the Lipsciz constants of different layers [Pang *et al.*, 2025]. In summary, QAT lacks the mechanism to "absorb" the perturbations (or errors 1) in each layer of the network caused by the above three aspects.

As a result, even minor perturbations would lead to a substantial drop in performance, which is demonstrated as the poor generalization ability. As shown in Fig. 1, the instability leads a quantizated model to converge to a local sharp minima [Deng *et al.*, 2024]. Concretely, the sharp minima in the landscape illustrates that the network weight is almost only applicable to the current samples.

Based on the above analysis, we propose Feature-Perturbed Quantization (FPQ) that leverages implicit-regularization on hessian matrix to smooth the loss landscape for overcoming the instability problem. Intuitively, the perturbation makes the optimization of the weights perform well on the nearby result rather than exactly the current one. Consequently, we control perturbations of features in each layer during the training stage by encouraging the model to converge to flat minima. Besides, we theoretically discover the advantage of Stochastic Feature Perturbations (SFP), and why SFP should be combined with a feature distillation technique. Our contributions are as follows:

 Mathematically, we show that the performance drop caused by quantization error is highly related to the norm of Hessian, which is also mentioned empirically in [Deng et al., 2024]. Furthermore, we discover that

- minimizing perturbations in the feature of each layer implicitly minimizes this term. Theoretically, it is shown that adding noise to features can explicitly optimize the flatness of the model and improve the generalization ability of the model.
- We propose a approach to overcome the instability of QAT by leveraging implicit Hessian regularization. Instead of simply adding perturbations to the weights, we formulate the smoothness of landscape as the minimization of stochastic perturbation in feature, defined as the expected loss within the neighborhood of current neural network parameters. We theoretically discover the advantage of Stochastic Feature Perturbations (SFP), and why SFP should be combined with a feature distillation technique which leads to the improved performance.
- The proposed methods consistently improve QAT-based methods and match or improve the SOTA results on various network architectures on the CIFAR-10 and CIFAR-100. Besides, extensive experiments show that our methods outperform other QAT approaches.

2 Related Work

2.1 Quantization-Aware Training

As discussed in Section 1, the errors of the first two dimensions are related to QAT, while the third one pertains to the process of pre-training FP models, which is not the focus of this paper.

In the first dimension, the instability is attributed to biased backpropagated gradients due to the round operation. For instance, Straight-Through Estimator (STE) [Bengio et al., 2013] utilized the expected probability of stochastic quantization as the gradient value for the backpropagation. The EWGS [Lee et al., 2021] adaptively adjusted the quantized gradients of the quantization error, thereby compensating for the biased gradient. The PSG [Kim et al., 2020] scaled the gradients based on the position of the weight, effectively offering a form of gradient compensation. The instability of gradients also leads to the oscillation problem during the QAT learning process. The DiffQ [Défossez et al., 2021] identified that STE would lead to weight oscillations during training. The Overcoming Oscillation Quantization (OOQ) [Nagel et al., 2022] addressed the oscillation issues by encouraging the latent weights to align closely with the center of the quantization bin. The Resilient Binary Neural Network (ReBNN) [Xu et al., 2023] introduced a weighted reconstruction loss to formulate an adaptive training objective.

In the second dimension, DQ [Lin et al., 2019] controled the error in feature transmission by managing the Lipschitz constant. NIPQ [Shin et al., 2023] employed pseudo-quantization noise to simulate the quantization process, reducing quantization errors. Similarly, some PTQ efforts aligned with the features of the FP model through layer-wise [Nagel et al., 2020] and block-wise [Li et al., 2021a], [Wei et al., 2022] reconstruction, thereby preventing the further propagation of errors within the network. To the best of our knowledge, we are the first to apply this idea to stabilize the QAT.

¹if it doesn't cause confusion, we will abuse use these terms.

Specially, for the quantization of Stable Diffusion (SD), the phenomenon of error accumulation is more pronounced due to the multi-step inference of the denoising process. BitsFusion [Sui et al., 2024] employs a mixed-precision approach to mitigate the accumulation of errors during the denoising process. Moreover, most of the work on SD quantization [Li et al., 2023a], [Huang et al., 2024], [He et al., 2024], [So et al., 2024] is based on BRECQ, as the block-wise reconstruction in BRECQ can minimize error propagation as much as possible. However, this work differs from their focus. Their concern is addressing the accuracy issues caused by error accumulation, while we are concerned with the instability issues arising from error propagation.

2.2 **Adversarial Robustness**

In this paper, we argue that QAT should exhibit robustness against feature perturbations. This aim aligns with the topic of adversarial robustness, which focused on mitigating the vulnerability of neural networks to the perturbations from input [Szegedy, 2013], e.g., random smoothing [Lecuyer et al., 2019], [Cohen et al., 2019], and adversarial training [Goodfellow et al., 2014], [Madry et al., 2017]. Adversarial training, in particular, optimized the worst-case training loss and has been shown to not only improve robustness but also enhanced performance in tasks such as image classification [Xie et al., 2020]. To the best of our knowledge, we are the first to apply this idea to stabilize QAT.

Proposed Method

3.1 **Notation and Background**

Basic Notations. In this paper, x represents a matrix (or tensor), a vector is denoted as x, f(x; w) represents a FP model with the weight w and the input x, f(x; w, s, z) represents a quantized model with the parameter w, quantization parameter s, z and the input x. We assume sample x is generated from the training set \mathcal{D}_t .

Quantization. Step size s and zero point z serve as a bridge between floating-point and fixed-point representations. Given the input tensor x^2 , the quantization operation is as follows:

$$\mathbf{x}_{int} = clip\left(\lfloor \frac{\mathbf{x}}{\mathbf{s}} \rceil + \mathbf{z}, 0, 2^{q} - 1\right),$$

$$\hat{\mathbf{x}} = (\mathbf{x}_{int} - \mathbf{z})\mathbf{s},$$
(3)

where $|\cdot|$ represents the rounding-to-nearest operator, q is the predefined quantization bit-width, s denotes the scale between two subsequent quantization levels. z stands for the zero-points. Both s and z are initialized by a calibration set \mathcal{D}_c from the training dataset \mathcal{D}_t , i.e., $\mathcal{D}_c \in \mathcal{D}_t$.

$$s = \frac{x_{max} - x_{min}}{2^q - 1},$$

$$z = \lfloor q_{max} - \frac{x_{max}}{s} \rceil,$$
(4)

$$z = \lfloor q_{max} - \frac{x_{max}}{s} \rceil, \tag{5}$$

where q_{max} is the maximum value of the quantized integer.

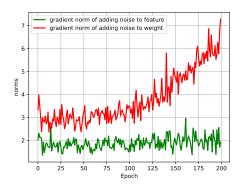


Figure 2: A comparison of the norm $\|\nabla_{\boldsymbol{w}}L(\boldsymbol{w})\|$ trajectories of ResNet-18 on CIFIAR-10.

We follow the practice in LSQ [Esser et al., 2019], where s is a learnable parameter. Therefore, the loss function of a quantized model is given as follows:

$$\underset{\boldsymbol{w}.\boldsymbol{s}}{\operatorname{arg\,min}} \ \mathbb{E}_{\boldsymbol{x} \sim \mathscr{D}_t}[L\left(\boldsymbol{x}; \boldsymbol{w}, \boldsymbol{s}\right)], \tag{6}$$

where $L(\cdot; \cdot)$ is the predefined loss function.

Notice that, the zero-points z are initialized by (5) with the calibration set \mathcal{D}_c , and are fixed throughout the entire QAT training process. During QAT training, the weights involved in the forward propagation are actually the quantized weights \hat{w} , rather than the floating-point weights w.

Feature-Perturbation brings Implicit Regularization on Hessian Matrix

Motivation.

The convergence property of oscillation near the target value is greatly beneficial to enhance the robustness of the network [Chen and Hsieh, 2020]. When some perturbation δ exists, the objective function can be approximated via Taylor expansion as follows:

$$\mathbb{E}[L(\boldsymbol{w} + \boldsymbol{\delta})]$$

$$\approx \mathbb{E}[L(\boldsymbol{w}) + \boldsymbol{\delta} \cdot \nabla_{\boldsymbol{w}} L(\boldsymbol{w}) + \frac{1}{2} \boldsymbol{\delta}^{T} \cdot \nabla_{\boldsymbol{w}}^{2} L(\boldsymbol{w}) \cdot \boldsymbol{\delta}]$$

$$\approx L(\boldsymbol{w}) + \mathbb{E}[\boldsymbol{\delta}] \cdot \nabla_{\boldsymbol{w}} L(\boldsymbol{w}) + \frac{\mathbb{E}[\boldsymbol{\delta}^{2}]}{2} \operatorname{Tr}(\nabla_{\boldsymbol{w}}^{2} L(\boldsymbol{w}))$$
(7)

where w is the weight of a DNN f(w). The third term of Eq. (7) involves the Hessian matrix's trace. [Keskar et al., 2017] and [Wen et al., 2020] verified that the smaller the trace of the Hessian matrix is, the flatter the landscape of loss is. A flat loss surface generally aids the model in finding good local optima to enhance the model's generalization capability.

We should make the second term in Eq. (7) be zero as follows:

$$\mathbb{E}[\boldsymbol{\delta}] \cdot \nabla_{\boldsymbol{w}} L(\boldsymbol{w}) = 0. \tag{8}$$

There are two conditions make the Eq.(8) be as zero as pos-

• Condition 1: The $\nabla_{\boldsymbol{w}} L(\boldsymbol{w})$ should be close enough to

²It could either be feature x or weight w.

• Condition 2: The expectation of perturbation $\mathbb{E}[\delta]$ of every layer should be zero.

Intuitively, when a well-trained model f(x, w) is used to fine-tune the QAT model, the $\nabla_w L(w)$ would be nearly equal to zero. However, when a certain perturbation δ is injected into either the weight or the feature of each layer, a natural question is: which scheme would incur a smaller norm of the gradient $\nabla_w L(w)$ than the other?

Therefore, we investigated the norm of the gradient $\nabla_{\boldsymbol{w}}L(\boldsymbol{w})$ when the perturbation $\boldsymbol{\delta}$ is injected into either the weight or the feature of resnet-18 model on the CIFAR-10 dataset. Results in Fig. 2 show that the norm of the gradient norm $\|\nabla_{\boldsymbol{w}}L(\boldsymbol{w})\|$ caused by the weight perturbation is larger than that of the feature perturbation. Therefore, in our work, we only apply perturbations to the features.

Feature Perturbation Quantization

Feature Perturbation Quantization (FPQ) introduces the perturbations into features, pushing the quantized model to live at a flat local minima. Without loss of generality, taking DNN as an example, we assume that a network has N convolutional layers. Given the input sample \boldsymbol{x} , the inputs of each layer for a quantized model are represented as, $\{\boldsymbol{x}_s^1, \boldsymbol{x}_s^2, \dots, \boldsymbol{x}_s^N\}$. We apply perturbations to the inputs of each convolutional layer of quantized model as follows:

$$\boldsymbol{x}_{s}^{l} = \boldsymbol{x}_{s}^{l} + \boldsymbol{\delta}, \boldsymbol{\delta} \sim U[-\frac{\boldsymbol{s}^{l}}{2}, \frac{\boldsymbol{s}^{l}}{2}]$$
 (9)

where \boldsymbol{x}_s^l is the input feature of the l-th layer of quantized model, $\boldsymbol{\delta}$ is the injected perturbation which follows a uniform distribution $U[-\frac{s^l}{2},\frac{s^l}{2}]$, and \boldsymbol{s}^l is the quantization parameter scale corresponding to the input feature \boldsymbol{x}^l . However, simply injecting perturbations by FPQ could disrupt the features of each layers of DNN, empirically resulting in inferior results.

Proposition 1 discovers that if w^l represents the weights of the l-th convolutional layer and x^l is the corresponding input feature, the expected perturbation $\mathbb{E}[\delta]$ is always biased.

Proposition 1. (Inject noise into multiple layers would result in a biased expectation) Without loss of generality, given a DNN with $N(N \geq 2)$ layers, if noises $\delta^l(1 \leq l \leq N)$ are simultaneously injected into different layers, the accumulated perturbation from different layers is biased.

Proof. Without loss of generality, a DNN is represented as

$$f_N(\boldsymbol{x}) = (\phi_N \dots \circ \phi_l \circ \dots \circ \phi_0)(\boldsymbol{x}), \tag{10}$$

where ϕ_l could be any module of the neural network, e.g., conventional layer, attention layer.

For the l-th layer, the perturbation comes from two sources: the first one is the perturbation δ^l that we directly injected by Eq. (9); and the second one is from the perturbation propagated from the last layer ϕ_{l-1} . Therefore, the expectation of the perturbation of the l-th layer $\mathbb{E}\left(\delta_{\text{total}}\right)$ is as follows:

$$\mathbb{E}\left(\boldsymbol{\delta}_{\text{total}}\right)$$

$$= \mathbb{E}\left[\boldsymbol{\delta}^{l} + f_{l-1}\left(\boldsymbol{x}^{l-1} + \boldsymbol{\delta}^{l-1}\right) - f_{l-1}\left(\boldsymbol{x}^{l-1}\right)\right]$$

$$= \mathbb{E}\left(\boldsymbol{\delta}^{l}\right) + \mathbb{E}\left[f_{l-1}\left(\boldsymbol{x}^{l-1} + \boldsymbol{\delta}^{l-1}\right) - f_{l-1}\left(\boldsymbol{x}^{l-1}\right)\right].$$
(11)

The first term in Eq. (11) is a uniform distribution with a expectation of $\mathbb{E}\left(\boldsymbol{\delta}^{l}\right)=0$. Consequently, we have:

$$\mathbb{E}\left(\boldsymbol{\delta}_{\text{total}}\right) = \mathbb{E}\left[\left(f_{l-1}\left(\boldsymbol{x}^{l-1} + \boldsymbol{\delta}^{l-1}\right) - f_{l-1}\left(\boldsymbol{x}^{l-1}\right)\right)\right].$$
(12)

Assuming that the function f_{l-1} is smooth at the point x^{l-1} , and that the perturbation δ^{l-1} is NOT sufficiently small, we apply the second-order Taylor approximation to Eq. (12) as follows:

$$\mathbb{E}\left(\delta_{\text{total}}\right)$$

$$\approx \mathbb{E}\left[\nabla f_{l-1}(\boldsymbol{x}^{l-1})^T \boldsymbol{\delta}^{l-1} + \frac{1}{2}(\boldsymbol{\delta}^{l-1})^T \nabla^2 f_{l-1}(\boldsymbol{x}^{l-1}) \boldsymbol{\delta}^{l-1}\right]$$

$$= \mathbb{E}\left[\frac{1}{2}(\boldsymbol{\delta}^{l-1})^T \nabla^2 f_{l-1}(\boldsymbol{x}^{l-1}) \boldsymbol{\delta}^{l-1}\right] \neq 0.$$
(13)

To reduce the bias, we propose a Stochastic Feature Perturbations (SFP) with a predefined probability p(p>0). Concretely, the l-th features \boldsymbol{x}^l is stochastically injected noise as follows:

$$\boldsymbol{x}_{s}^{l} = \boldsymbol{x}_{s}^{l} + \boldsymbol{\delta}$$
, with probability p . (14)

With SFP, the probability of injecting perturbations into all layers simultaneously is p^N , which significantly reduces the occurrence of the bias in Eq. (13), e.g., $0.1^{10}=1e-11$ for a DNN with 10 layers. Besides, we combined with a feature distillation called Channel-wise Standardization Distillation (CSD) to make the Condition 1 hold.

Channel-wise Standardization Distillation

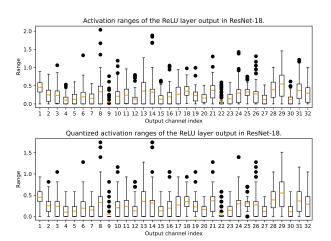


Figure 3: Comparisons of the output feature of the ResNet-18 before and after quantization. The orange line represents the mean value of the feature (best viewed in color).

We have observed that the quantization operation can affect the distribution of features. We visualized the output features of a ReLU layer in the ResNet-18 model to compare the changes in features before and after quantization. The results are shown in Fig. 3. The findings indicate that the

quantization operation can cause a shift in the distribution. Specifically, in Fig. 3, the feature with index 30 had a mean value of 0.12 before quantization, while after quantization, the mean value shifted to 0.11, resulting in a relative error of nearly 10%. The drifted distribution is unfriendly for distillation [Nagel et al., 2019b] [He et al., 2024]. In this work, To mitigate drifted distribution caused by quantization, we standardize features before distillation for forcing Mean Squared Error (MSE) to focus the feature distribution rather than the absolute values as follows:

$$\tilde{z}^{l} = Norm(z^{l}) = \frac{z^{l} - \mu(z^{l})}{\sqrt{\sigma^{2}(z^{l}) + \epsilon}},$$
(15)

where z^l is the output of the l-th layer, \tilde{z}^l is the normalized feature, $\mu\left(z^l\right)$ is the mean of feature x^l , $\sigma^2\left(z^l\right)$ is the variance of the feature, and ϵ is the constant preventing the denominator being 0.

The student model (quantized) $f_S\left(\boldsymbol{x};\boldsymbol{w}_s,s_s,z_s\right)$ is initialized with a calibration dataset, while the teacher model (FP) $f_T\left(\boldsymbol{x};\boldsymbol{w}_t,s_t,z_t\right)$ serves as a reference. The standardized outputs of the l-th layer in the quantized model and that of the FP model are as follows:

$$\tilde{\mathbf{z}}_{s}^{l} = Norm(\hat{\mathbf{w}}_{s}^{l}\mathbf{x}_{s}^{l}),
\tilde{\mathbf{z}}_{t}^{l} = Norm(\mathbf{w}_{t}^{l}\mathbf{x}_{t}^{l}),$$
(16)

where \tilde{z}_s^l and \tilde{z}_t^l are the standardized features of the l-th layer of the quantized model and the FP one, respectively.

To make Condition 1 hold, one reasonable assumption is that if the output of student model $f_S\left(\boldsymbol{x};\boldsymbol{w}_s,\boldsymbol{s}_s,\boldsymbol{z}_s\right)$ is equal to that of the teacher one $f_T\left(\boldsymbol{x};\boldsymbol{w}_t,\boldsymbol{s}_t,\boldsymbol{z}_t\right)$, the gradient $\nabla_{\hat{\boldsymbol{w}}}L(\hat{\boldsymbol{w}})$ tends to be zero. The CSD is as follows:

$$L_{CSD} = \sum_{i \in [1,N]} \sum_{j \in [1,c]} \left\| \tilde{z}_t^{i;j} - \tilde{z}_s^{i;j} \right\|_2^2, \tag{17}$$

where N represents the number of layers, c represents the number of channels output by the i-th convolution, $\tilde{z}_s^{i;j}$, $\tilde{z}_t^{i;j}$ represent the standardized features of the j-th channel of the i-th convolution of the quantized model and the FP model, respectively, $\|\cdot\|_2$ denotes ℓ_2 normalization.

3.3 Implicit Regularization on Hessian Matrix

In the following, we first explain why the spectral norm of Hessian is correlated with solution quality, and then formally show that the difference of our algorithms with Sharpness-aware Minimization (SAM).

Why is Hessian norm correlated with solution quality?

Assume w^* is the optimal weight of Eq. (6). Based on Taylor expansion and assume $\nabla L_{\rm val}(w^*) = 0$ due to optimality condition, we have

$$L_{\text{val}}(\hat{\boldsymbol{w}}) = L_{\text{val}}(\boldsymbol{w}^*) + \frac{1}{2}(\hat{\boldsymbol{w}} - \boldsymbol{w}^*)^T \hat{H}(\hat{\boldsymbol{w}} - \boldsymbol{w}^*), \quad (18)$$

where $\hat{H} = \int_{\boldsymbol{w}^*}^{\hat{\boldsymbol{w}}} \nabla^2 L_{\text{val}}(\boldsymbol{w}) d\boldsymbol{w}$ is the average Hessian. If we assume that Hessian is stable in a local region, then the quantity of $C = \|\nabla^2 L_{\text{val}}(\boldsymbol{w}^*)\| \|\hat{\boldsymbol{w}} - \boldsymbol{w}^*\|$ can approximately bound the performance drop when projecting \boldsymbol{w}^* to $\hat{\boldsymbol{w}}$. After

fine tuning, if $\hat{\boldsymbol{w}}$ is the new optimal weight vector, we expect $L_{\text{val}}(\hat{\boldsymbol{w}})$ to be smaller than $L_{\text{val}}(\boldsymbol{w}^*)$, provided that the training and validation losses are highly correlated. Therefore, the performance of $L_{\text{val}}(\hat{\boldsymbol{w}})$, which is the quantity that we care for, will also be bounded by C. Note that the bound C could be quite loose since that the network weights changed when transitioning from \boldsymbol{w}^* to $\hat{\boldsymbol{w}}$. A more precise bound can be obtained by treating $g(\boldsymbol{w}) = L_{\text{val}}(\boldsymbol{w})$ as a function only parameterized by \boldsymbol{w} , and then calculate its derivative/Hessian by implicit function theory.

The difference between our method and SAM. The concept of searching for minima characterized as "flat minima" was introduced in [Hochreiter and Schmidhuber, 1994] and extensive research has been conducted to explore its connection with the generalization ability [Andriushchenko and Flammarion, 2022] [Zhang et al., 2021]. SAM [Foret et al., 2020] enhances the generalization ability of the model as follows:

$$\min_{\boldsymbol{w}} \quad L^{SAM}(\boldsymbol{w}) + \lambda \|\boldsymbol{w}\|^2,$$
where
$$L^{SAM}(\boldsymbol{w}) = \max_{\|\boldsymbol{\epsilon}\| \le \rho} L(\boldsymbol{w} + \boldsymbol{\epsilon}),$$
(19)

in which ϵ represents weight perturbations in an Euclidean ball within the radius ρ , L^{SAM} is the perturbed loss, and $\lambda \| \boldsymbol{w} \|^2$ is the standard L2 norm.

In contrast, the proposed FPQ is formally defined as follows:

$$\begin{split} \min_{\boldsymbol{w}} \quad L_{\boldsymbol{\epsilon} \sim U[-\frac{s^l}{2}, \frac{s^l}{2}]}(\boldsymbol{w}; \boldsymbol{x}^l + \boldsymbol{\epsilon}), \\ s.t. \quad \mathbb{E}[\boldsymbol{\delta}] \cdot \nabla_{\boldsymbol{w}} L(\boldsymbol{w}) = 0, \end{split} \tag{20}$$

where x^l is the input feature of the l-th layer in a DNN.

Table 1: The comparison of results for optimizing LSQ using SAM and FPQ, and the accuracy (%) of the model with W4A4 quantization on the CIFAR-10 dataset.

Methods	Res18	MBV2
Full prec.	88.72	85.81
LSQ+SAM	89.75	84.72
FPQ	90.16	85.53

Rather than directly perturbing the weight in Eq. (19), we instead perturbing the features through Eq. (9). The comparison of results between FPQ and SAM is shown in Tab. 1. As discussed in Eq. (7), FPQ imposes an implicit regularization on the Hessian matrix. The results indicate that the optimization using SAM performs worse than that using FPQ. One possible reason is that in high-dimensional spaces, there are many directions of perturbations δ and their size ρ to be chosen, and the random approach in FPQ may outperform the method of selecting the largest perturbation in SAM for QAT.

3.4 Training Processing

Given a labeled sample (X,y) and the corresponding label y, the output of the quantized model and the FP model are:

$$z_s^o = f_S(\mathbf{x}; \hat{\mathbf{w}}_s, \mathbf{s}_s), z_t^o = f_T(\mathbf{x}; \hat{\mathbf{w}}_t, \mathbf{s}_t).$$
(21)

Algorithm 1 QAT with FPQ

- 1: **Input:** labeled data X; FP model f(x; w)
- 2: for i = 1 to \cdots do
- 3: Feed the X into models based on Eq. (21), while injecting perturbations into all layers of a DNN with probability p by Eq. (14);
- 4: Obtain and standarize the outputs of each layer of the quantized model and the FP model based on Eq. (16);
- 5: Update for student model based on Eq. (17) and Eq. (22);
- 6: end for
- 7: **Output:** $f_S(x; w_s, s_s, z_s)$.

In the forward through Eq. (21), we apply with stochastic perturbation δ in all the input of convolutional layer with a predefined probability p. The perturbation drawn from a uniform distribution through Eq. (9).

In this paper, we focus on the classification task. Therefore, the whole loss consists of two components as follows:

$$L_{total}\left(\hat{\boldsymbol{w}}, \boldsymbol{x}\right) = CE\left(\boldsymbol{z}_{s}^{o}, y\right) + L_{CSD}, \tag{22}$$

where $CE\left(\cdot,\cdot\right)$ denotes the cross-entropy loss for classification tasks, z_{o} presents the output from the quantized model for the labeled data (X,y). Training procedure is shown in Algorithm 1.

4 Experiments

Experimental Protocols and Datasets. Our code is based on PyTorch [Paszke et al., 2019] and relies on the MQBench [Li et al., 2021b] package. We used asymmetric quantization by default. In this paper, we used the CIFAR-10 and CIFAR-100 [Krizhevsky et al., 2009] as dataset. We randomly selected 100 images for CIFAR-10 and CIFAR-100 as the calibration set. We also kept the first and last layers with 8-bit quantization, the same as QDrop [Wei et al., 2022]. Additionally, we employed per-channel quantization for weight quantization. We used WXAX to represent X-bit weight and activation quantization.

Training Details. We used SGD as the optimizer, with a batch size of 256 and a base learning rate of 0.01. The default learning rate (LR) scheduler followed the cosine annealing method. The weight decay was 0.0005, and the SGD momentum was 0.9. We trained for 200 epochs otherwise specified.

Table 2: Ablation studies of perturbation and CSD (Accuracy %) on CIFAR-10 with W2A4 quantization.

Perturbations	CSD	ResNet-18
		88.36
\checkmark		89.30
	\checkmark	89.66
√	✓	89.92

4.1 Ablation Study

Effectiveness of probability FPQ. To investigate the impact of FPQ, we conducted ablation experiments to validate the

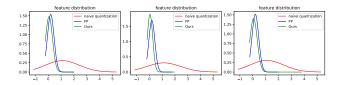


Figure 4: Feature distributions of the FP ResNet-18 (blue lines), native baseline (LSQ, red lines), and ours method (green lines) for the same feature of ResNet-18 model on CIFAR-10. We random select three samples and plot the output feature of the same layer.

effects of the perturbation and L_{CSD} . We used the W2A4 model of ResNet-18 [He *et al.*, 2016] with the LSQ method as the baseline, which achieved an accuracy of 88.36% on CIFAR-10 dataset. Tab. 2 illustrated that FPQ has improved the accuracy of W2A4 quantized models for ResNet architectures. Adding only the perturbation in Eq. (14) improved the baseline by 0.94%, using only CSD improved the baseline by 1.3%, and when both were used together, the result was better, improving the baseline by 1.56%.

Table 3: The effectiveness of the probability p on CIFAR-10 with W2A4 quantization (Accuracy %).

<i>p</i> of FPQ in Eq. (14)	Val acc (%)
0	89.66
0.1	89.92
0.3	89.90
0.5	89.83
0.7	89.59
0.9	89.68
1	89.48

Effectiveness of probability p. To investigate the impact of probability p in Eq. (14), we used CIFAR-10 as the dataset. Tab. 3 illustrated that the performances of the W2A4 model with the seven different sets of p. The experimental results indicated that when the random probability p is too high, excessive perturbations can disrupt the local minima of the quantized model. Conversely, when the perturbations are too small, the insufficient noise failed to smooth the sharpness of the model's loss landscape. An optimal probability p lies within the range of 0.1 to 0.5.

4.2 Literature Comparison

We selected ResNet-18 and ResNet-50 [He *et al.*, 2016], MobileNetV1 [Howard *et al.*, 2017] and MobileNetV2 [Sandler *et al.*, 2018] with depth-wise separable convolutions as the representative network architectures.

CIFAR-10. In Tab. 4, we quantized the weights and activations to 2-bit and 4-bit. We compared our approach with the effective baselines, including LSQ [Esser et al., 2019], LSQ+ [Bhalgat et al., 2020], PACT [Choi et al., 2018] and KD [Hinton et al., 2015]. Tab. 4 illustrated that when the entire training set of CIFAR-10 is used, FPQ significantly surpassed the baselines. In W4A4 quantization, FPQ achieved about 1~2% accuracy improvements over LSQ. Furthermore, to explore the ability of FPQ, we conducted W2A4 and

Table 4: Comparison among different QAT strategies in terms of accuracy on CIFAR-10.

Labeled data	Methods	W/A	Res18	Res50	MBV1	MBV2
50000	Full Prec.	32/32	88.72	89.95	85.52	85.81
	PACT [Choi et al., 2018]	4/4	88.15	85.27	80.77	79.88
	LSQ [Esser et al., 2019]	4/4	86.69	90.01	82.39	84.45
	LSQ+ [Bhalgat et al., 2020]	4/4	88.40	90.30	84.32	84.30
	KD [Hinton et al., 2015]	4/4	88.86	90.34	84.77	83.79
	FPQ (Ours)	4/4	90.16	90.62	84.94	85.53
	PACT [Choi et al., 2018]	2/4	87.55	85.24	69.04	67.18
50000	LSQ [Esser et al., 2019]	2/4	88.36	90.01	78.15	78.15
50000	LSQ+ [Bhalgat et al., 2020]	2/4	87.76	89.62	81.26	77.00
=	KD [Hinton et al., 2015]	2/4	88.83	90.18	78.84	75.56
	FPQ (Ours)	2/4	89.92	90.39	81.45	79.33
	PACT [Choi et al., 2018]	2/2	76.90	64.94	11.71	10.58
	LSQ [Esser et al., 2019]	2/2	87.60	87.79	75.29	70.32
	LSQ+ [Bhalgat et al., 2020]	2/2	87.60	86.10	74.22	72.18
	KD [Hinton et al., 2015]	2/2	88.06	89.20	68.62	67.15
	FPQ (Ours)	2/2	88.11	89.40	76.25	73.00

Table 5: Comparison among different QAT strategies regarding accuracy on CIFAR-100.

Labeled data	Methods	W/A	Res18	Res50	MBV1	MBV2
50000	Full Prec.	32/32	75.40	78.94	70.22	71.30
	PACT [Choi et al., 2018]	4/4	74.17	74.78	64.65	64.06
	LSQ [Esser et al., 2019]	4/4	75.30	78.20	68.63	69.01
	LSQ+ [Bhalgat et al., 2020]	4/4	74.50	77.39	67.89	68.25
	KD [Hinton et al., 2015]	4/4	74.70	78.80	70.96	71.66
	FPQ (Ours)	4/4	75.84	78.8	67.55	68.24
	PACT [Choi et al., 2018]	2/4	73.77	74.72	49.98	57.90
50000	LSQ [Esser et al., 2019]	2/4	74.93	77.82	65.13	66.15
30000	LSQ+ [Bhalgat et al., 2020]	2/4	73.90	76.61	65.28	66.24
	KD [Hinton et al., 2015]	2/4	74.35	77.34	66.90	63.77
LSQ [Esser et al., 20 LSQ+ [Bhalgat et al	FPQ (Ours)	2/4	75.77	78.11	64.68	65.35
	PACT [Choi et al., 2018]	2/2	65.16	4.26	3.25	8.39
	LSQ [Esser et al., 2019]	2/2	71.80	62.79	55.53	31.08
	LSQ+ [Bhalgat et al., 2020]	2/2	71.25	64.21	55.56	30.08
	KD [Hinton et al., 2015]	2/2	73.13	63.16	55.37	28.56
	FPQ (Ours)	2/2	71.73	65.23	58.46	33.16

W2A4 quantization experiments. In W2A4 quantization, FPQ consistently achieved a $1\sim2\%$ accuracy improvement over LSQ in Tab. 4. In W2A2 setting, FPQ achieved about $1\sim3\%$ accuracy improvements over LSQ. Moreover, there are two interesting observations as follows:

- For W4A4, our method significantly surpassed the FP counterparts for both ResNet-18 and ResNet-50. For example, on the ResNet-18 model, FPQ surpassed the FP model by 1.44% in accuracy, and on the ResNet-50 model, FPQ exceeded the FP model by 0.67%.
- From W4A4 to W2A2, the performance drop of our method is significantly lower that the other SOTA methods. For instance, on the ResNet-50 model, the LSQ method decreased by 2.22% when reducing from W4A4 to W2A2, while FPQ decreased by 1.22%. On the MobileNetV1 model, the LSQ+ method saw a 10.1% drop when going from W4A4 to W2A2, while FPQ decreased by 8.69%

CIFAR-100. In Tab. 5, we evaluate quantization performance across varying bit-widths (W4A4, W2A4, W2A2) on CIFAR-100. Same to CIFAR-10, FPQ demonstrates superior performance in most scenarios. For W4A4 quantization, FPQ achieves the highest accuracy on ResNet-18 (75.84%) and ResNet-50 (78.8%), surpassing LSQ by 0.54%

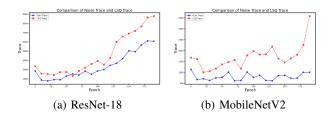


Figure 5: Trajectory of the Hessian matrix trace for ResNet-18 and MobileNetV2 models on the CIFAR-10 dataset.

and 0.6% respectively. Notably, FPQ even exceeds the full-precision baseline by 0.44% on ResNet-18. In W2A4 settings, FPQ maintains strong performance with ResNet-18 (75.77%) and ResNet-50 (78.11%), outperforming LSQ by 0.84% and 0.29%. For the challenging W2A2 configuration, FPQ achieves the best results on ResNet-50 (65.23%), MobileNetV1 (58.46%), and MobileNetV2 (33.16%), demonstrating robustness under extreme quantization.

4.3 Characteristics of FPQ

Generalization of FPQ: It has been empirically pointed out that the dominant eigenvalue of $\nabla^2 L_{\rm val}(w)$ (spectral norm of Hessian) is highly correlated with the generalization quality of QAT solutions [Keskar et al., 2017] [Wen et al., 2020]. In standard QAT training, the Hessian norm is usually great, which leads to deteriorating (test) performance of the solutions. In Fig. 5(a) and Fig. 5(b), we plot the Hessian trace during the training procedure and find that the Hessian trace of the proposed methods is significantly lower than that of the LSQ. The results demonstrate that FPQ would reduce the trace of the Hessian matrix numerically, thereby enhancing the model's generalization ability.

Distribution Visualization of FPQ: We visualized the feature distribution before and after quantization and the FP model to explore whether FPQ could align the distribution of the quantized model with that of the FP model.

As shown in Fig. 4, there was a significant distribution drift between the naive quantization and the FP model. This problem is the key reason for the drop in performance of the quantized model. Our method effectively alleviated this problem. On the one hand, FPQ leveraged the feature distribution of the FP model as the ground truth, reducing the distribution drift caused by quantization. On the other hand, FPQ retained the original task loss, making stochastic perturbation in Eq. (14) to smooth the local minima.

5 Conclusion

In this paper, we propose the FPQ for QAT-based method. By applying perturbations to the features, FPQ introduces the implicit regularization to the Hessian matrix, enhancing the stability of the model. Specifically, the regularization is carried out with random smoothing. FPQ possesses a much smoother landscape and has the theoretical guarantee to regularize the Hessian norm of the validation loss. Extensive experiments have illustrate the effectiveness of FPQ and we outperform various SOTA methods.

References

- [Andriushchenko and Flammarion, 2022] Maksym Andriushchenko and Nicolas Flammarion. Towards understanding sharpness-aware minimization. In *International Conference on Machine Learning*, pages 639–668. PMLR, 2022.
- [Bengio *et al.*, 2013] Yoshua Bengio, Nicholas Léonard, and Aaron Courville. Estimating or propagating gradients through stochastic neurons for conditional computation. *arXiv preprint arXiv:1308.3432*, 2013.
- [Bhalgat et al., 2020] Yash Bhalgat, Jinwon Lee, Markus Nagel, Tijmen Blankevoort, and Nojun Kwak. Lsq+: Improving low-bit quantization through learnable offsets and better initialization. In *Proceedings of the IEEE/CVF Conference on Computer Vision and Pattern Recognition Workshops*, pages 696–697, 2020.
- [Chen and Hsieh, 2020] Xiangning Chen and Cho-Jui Hsieh. Stabilizing differentiable architecture search via perturbation-based regularization. In *International conference on machine learning*, pages 1554–1565. PMLR, 2020.
- [Choi et al., 2018] Jungwook Choi, Zhuo Wang, Swagath Venkataramani, Pierce I-Jen Chuang, Vijayalakshmi Srinivasan, and Kailash Gopalakrishnan. Pact: Parameterized clipping activation for quantized neural networks. arXiv preprint arXiv:1805.06085, 2018.
- [Cohen *et al.*, 2019] Jeremy Cohen, Elan Rosenfeld, and Zico Kolter. Certified adversarial robustness via randomized smoothing. In *international conference on machine learning*, pages 1310–1320. PMLR, 2019.
- [Défossez *et al.*, 2021] Alexandre Défossez, Yossi Adi, and Gabriel Synnaeve. Differentiable model compression via pseudo quantization noise. *arXiv preprint arXiv:2104.09987*, 2021.
- [Deng et al., 2024] Jiaxin Deng, Junbiao Pang, and Baochang Zhang. Asymptotic unbiased sample sampling to speed up sharpness-aware minimization, 2024.
- [Esser et al., 2019] Steven K Esser, Jeffrey L McKinstry, Deepika Bablani, Rathinakumar Appuswamy, and Dharmendra S Modha. Learned step size quantization. arXiv preprint arXiv:1902.08153, 2019.
- [Foret *et al.*, 2020] Pierre Foret, Ariel Kleiner, Hossein Mobahi, and Behnam Neyshabur. Sharpness-aware minimization for efficiently improving generalization. *arXiv* preprint arXiv:2010.01412, 2020.
- [Goodfellow *et al.*, 2014] Ian J Goodfellow, Jonathon Shlens, and Christian Szegedy. Explaining and harnessing adversarial examples. *arXiv preprint arXiv:1412.6572*, 2014.
- [Han *et al.*, 2015] Song Han, Huizi Mao, and William J Dally. Deep compression: Compressing deep neural networks with pruning, trained quantization and huffman coding. *arXiv preprint arXiv:1510.00149*, 2015.

- [He et al., 2016] Kaiming He, Xiangyu Zhang, Shaoqing Ren, and Jian Sun. Deep residual learning for image recognition. In *Proceedings of the IEEE conference on computer vision and pattern recognition*, pages 770–778, 2016.
- [He et al., 2024] Yefei He, Luping Liu, Jing Liu, Weijia Wu, Hong Zhou, and Bohan Zhuang. Ptqd: Accurate post-training quantization for diffusion models. Advances in Neural Information Processing Systems, 36, 2024.
- [Hinton *et al.*, 2015] Geoffrey Hinton, Oriol Vinyals, and Jeff Dean. Distilling the knowledge in a neural network. *arXiv preprint arXiv:1503.02531*, 2015.
- [Hochreiter and Schmidhuber, 1994] Sepp Hochreiter and Jürgen Schmidhuber. Simplifying neural nets by discovering flat minima. *Advances in neural information processing systems*, 7, 1994.
- [Howard *et al.*, 2017] Andrew G Howard, Menglong Zhu, Bo Chen, Dmitry Kalenichenko, Weijun Wang, Tobias Weyand, Marco Andreetto, and Hartwig Adam. Mobilenets: Efficient convolutional neural networks for mobile vision applications. *arXiv preprint arXiv:1704.04861*, 2017.
- [Huang et al., 2024] Yushi Huang, Ruihao Gong, Jing Liu, Tianlong Chen, and Xianglong Liu. Tfmq-dm: Temporal feature maintenance quantization for diffusion models. In *Proceedings of the IEEE/CVF Conference on Computer Vision and Pattern Recognition*, pages 7362–7371, 2024.
- [Keskar et al., 2017] Nitish Shirish Keskar, Dheevatsa Mudigere, Jorge Nocedal, Mikhail Smelyanskiy, and Ping Tak Peter Tang. On large-batch training for deep learning: Generalization gap and sharp minima. In *International Conference on Learning Representations*, 2017.
- [Kim et al., 2020] Jangho Kim, KiYoon Yoo, and Nojun Kwak. Position-based scaled gradient for model quantization and pruning. Advances in neural information processing systems, 33:20415–20426, 2020.
- [Krizhevsky *et al.*, 2009] Alex Krizhevsky, Geoffrey Hinton, et al. Learning multiple layers of features from tiny images. 2009.
- [Lecuyer *et al.*, 2019] Mathias Lecuyer, Vaggelis Atlidakis, Roxana Geambasu, Daniel Hsu, and Suman Jana. Certified robustness to adversarial examples with differential privacy. In *2019 IEEE symposium on security and privacy* (*SP*), pages 656–672. IEEE, 2019.
- [Lee et al., 2021] Junghyup Lee, Dohyung Kim, and Bumsub Ham. Network quantization with element-wise gradient scaling. In *Proceedings of the IEEE/CVF conference on computer vision and pattern recognition*, pages 6448–6457, 2021.
- [Li et al., 2021a] Yuhang Li, Ruihao Gong, Xu Tan, Yang Yang, Peng Hu, Qi Zhang, Fengwei Yu, Wei Wang, and Shi Gu. Brecq: Pushing the limit of post-training quantization by block reconstruction. arXiv preprint arXiv:2102.05426, 2021.
- [Li et al., 2021b] Yuhang Li, Mingzhu Shen, Jian Ma, Yan Ren, Mingxin Zhao, Qi Zhang, Ruihao Gong, Fengwei Yu,

- and Junjie Yan. Mqbench: Towards reproducible and deployable model quantization benchmark. *arXiv preprint arXiv:2111.03759*, 2021.
- [Li et al., 2023a] Xiuyu Li, Yijiang Liu, Long Lian, Huanrui Yang, Zhen Dong, Daniel Kang, Shanghang Zhang, and Kurt Keutzer. Q-diffusion: Quantizing diffusion models. In Proceedings of the IEEE/CVF International Conference on Computer Vision, pages 17535–17545, 2023.
- [Li et al., 2023b] Zhikai Li, Mengjuan Chen, Junrui Xiao, and Qingyi Gu. Psaq-vit v2: Toward accurate and general data-free quantization for vision transformers. IEEE Transactions on Neural Networks and Learning Systems, pages 1–12, 2023.
- [Lin *et al.*, 2019] Ji Lin, Chuang Gan, and Song Han. Defensive quantization: When efficiency meets robustness. *arXiv* preprint arXiv:1904.08444, 2019.
- [Madry *et al.*, 2017] Aleksander Madry, Aleksandar Makelov, Ludwig Schmidt, Dimitris Tsipras, and Adrian Vladu. Towards deep learning models resistant to adversarial attacks. *stat*, 1050(9), 2017.
- [Nagel et al., 2019a] Markus Nagel, Mart van Baalen, Tijmen Blankevoort, and Max Welling. Data-free quantization through weight equalization and bias correction. In *Proceedings of the IEEE/CVF International Conference on Computer Vision*, pages 1325–1334, 2019.
- [Nagel et al., 2019b] Markus Nagel, Mart van Baalen, Tijmen Blankevoort, and Max Welling. Data-free quantization through weight equalization and bias correction. In Proceedings of the IEEE/CVF International Conference on Computer Vision, pages 1325–1334, 2019.
- [Nagel et al., 2020] Markus Nagel, Rana Ali Amjad, Mart Van Baalen, Christos Louizos, and Tijmen Blankevoort. Up or down? adaptive rounding for post-training quantization. In *International Conference on Machine Learning*, pages 7197–7206. PMLR, 2020.
- [Nagel et al., 2022] Markus Nagel, Marios Fournarakis, Yelysei Bondarenko, and Tijmen Blankevoort. Overcoming oscillations in quantization-aware training. In *International Conference on Machine Learning*, pages 16318–16330. PMLR, 2022.
- [Pang *et al.*, 2025] Junbiao Pang, Tianyang Cai, Baochang Zhang, and Jiaqi Wu. In-distribution consistency regularization improves the generalization of quantization-aware training, 2025.
- [Paszke et al., 2019] Adam Paszke, Sam Gross, Francisco Massa, Adam Lerer, James Bradbury, Gregory Chanan, Trevor Killeen, Zeming Lin, Natalia Gimelshein, Luca Antiga, et al. Pytorch: An imperative style, high-performance deep learning library. Advances in neural information processing systems, 32, 2019.
- [Qian and Wegman, 2018] Haifeng Qian and Mark N Wegman. L2-nonexpansive neural networks. *arXiv preprint arXiv:1802.07896*, 2018.
- [Sandler et al., 2018] Mark Sandler, Andrew Howard, Menglong Zhu, Andrey Zhmoginov, and Liang-Chieh Chen.

- Mobilenetv2: Inverted residuals and linear bottlenecks. In *Proceedings of the IEEE conference on computer vision and pattern recognition*, pages 4510–4520, 2018.
- [Shin et al., 2023] Juncheol Shin, Junhyuk So, Sein Park, Seungyeop Kang, Sungjoo Yoo, and Eunhyeok Park. Nipq: Noise proxy-based integrated pseudo-quantization. In Proceedings of the IEEE/CVF Conference on Computer Vision and Pattern Recognition, pages 3852–3861, 2023.
- [So et al., 2024] Junhyuk So, Jungwon Lee, Daehyun Ahn, Hyungjun Kim, and Eunhyeok Park. Temporal dynamic quantization for diffusion models. Advances in Neural Information Processing Systems, 36, 2024.
- [Sui *et al.*, 2024] Yang Sui, Yanyu Li, Anil Kag, Yerlan Idelbayev, Junli Cao, Ju Hu, Dhritiman Sagar, Bo Yuan, Sergey Tulyakov, and Jian Ren. Bitsfusion: 1.99 bits weight quantization of diffusion model. *arXiv preprint arXiv:2406.04333*, 2024.
- [Szegedy, 2013] C Szegedy. Intriguing properties of neural networks. *arXiv preprint arXiv:1312.6199*, 2013.
- [Wei *et al.*, 2022] Xiuying Wei, Ruihao Gong, Yuhang Li, Xianglong Liu, and Fengwei Yu. Qdrop: Randomly dropping quantization for extremely low-bit post-training quantization. *arXiv preprint arXiv:2203.05740*, 2022.
- [Wen et al., 2020] Yeming Wen, Kevin Luk, Maxime Gazeau, Guodong Zhang, Harris Chan, and Jimmy Ba. An empirical study of stochastic gradient descent with structured covariance noise. In *International Conference on Artificial Intelligence and Statistics*, 2020.
- [Xie et al., 2020] Cihang Xie, Mingxing Tan, Boqing Gong, Jiang Wang, Alan L Yuille, and Quoc V Le. Adversarial examples improve image recognition. In *Proceedings of the IEEE/CVF conference on computer vision and pattern recognition*, pages 819–828, 2020.
- [Xu et al., 2023] Sheng Xu, Yanjing Li, Teli Ma, Mingbao Lin, Hao Dong, Baochang Zhang, Peng Gao, and Jinhu Lu. Resilient binary neural network. In Proceedings of the AAAI Conference on Artificial Intelligence, volume 37, pages 10620–10628, 2023.
- [Zhang et al., 2021] Chiyuan Zhang, Samy Bengio, Moritz Hardt, Benjamin Recht, and Oriol Vinyals. Understanding deep learning (still) requires rethinking generalization. *Communications of the ACM*, 64(3):107–115, 2021.
- [Zhu et al., 2019] Shilin Zhu, Xin Dong, and Hao Su. Binary ensemble neural network: More bits per network or more networks per bit? In *Proceedings of the IEEE/CVF conference on computer vision and pattern recognition*, pages 4923–4932, 2019.
- [Zoph and Le, 2016] Barret Zoph and Quoc V Le. Neural architecture search with reinforcement learning. *arXiv* preprint arXiv:1611.01578, 2016.